Hindawi
Shock and Vibration
Volume 2021, Article ID 9994904, 11 pages
https://doi.org/10.1155/2021/9994904

Research Article

A Study on the Impact of Longwall-Mining Operation on the Stability of a Slope-Pillar Structure

Wenyong Bai,[1,2,3] **Jie Zhang**,[1,3] **Bin Wang**,[1,3] **Jianchen Zhang**,[1,3] **Hongru Li**,[1,3] **and Sen Yang**[1,3]

[1]*School of Energy Engineering, Xi'an University of Science and Technology, Xi'an 710054, Shaanxi, China*
[2]*School of Coal Engineering, Shanxi Datong University, Datong 037000, Shanxi, China*
[3]*Key Laboratory of Western Mine Exploitation and Hazard Prevention of Ministry of Education, Xi'an University of Science and Technology, Xi'an 710054, Shaanxi, China*

Correspondence should be addressed to Wenyong Bai; dtdxbwy@163.com

Received 31 March 2021; Revised 15 April 2021; Accepted 21 May 2021; Published 31 May 2021

Academic Editor: Thanh-Phong Dao

The slope-pillar structure is defined as an artificial construction shaped by a surface highwall mining and an underground longwall mining. In order to study the impact of stress variations (induced by the longwall-mining operations) on the stability of a slope-pillar structure, No. 30101-1 working face of Nanliang Coal Mine was selected as the study subject. A series of analysis including physical similar simulation test and the theoretical analysis were conducted to study the movement pattern of the overlying strata in the working face of the slope and the loading and the stability of the pillar column revealing the mechanism of dynamic load instability of nonuniformly distributed load "slope pillar." A "slope-pillar" reverse sliding structural model was proposed along with a newly established "slope-pillar" structural mechanical model and a formula to calculate the boundary width of the protection for the pillar under the extreme balance conditions. According to the study, the width of the protective pillar is designed at 20 m, and the roadway deformation during the working face and the stability of the pillar can satisfy the safety requirement concerning the working face, which further validates the theoretic deduction formula.

1. Introduction

The Shenfu-Dongsheng Coal Field, as an important coal energy base in China, is featured with shallow coal seams and diverse topography. Since the early 1990s, scholars have conducted a series of studies on shallow coal seam mining. The authors of [1–6] conducted a large number of on-site monitoring and tests to determine the mine pressure, the fracture law of the overlying strata, and strata control. Due to the staggered surface ravines in the western region, the drastic variance in the occurrence of slopes, and the interaction between the special topography and the shallow coal seam mining, a series of new features such as the appearance of underground pressure and the movement of the overburden at the working face were identified. Regarding the mining pressure and strata control under the special topography, Xufeng et al. adopted the roof structural study to the coal seaming under the slope of bedrock and sandy soil, resulting in the establishment of the depth of gully slope and the impacts of the slope angle on the mining pressure of the working face [7]. Taking the coal seam conditions under the Shenfu-Dongsheng Coal Field into account, Zhang et al. conducted simulation and concluded that a greater load from the working force was imposed on the upper slope as the depth of the gully slope increased [8–10]. Hu et al. suggested that several factors including the existence of the key strata, the depth of trench, and slope angle tended to influence the generation of dynamic loading pressure on the working face [11]. Wang et al. established a "support-surrounding rock" model under the gully in combination with the geological conditions of the mine and identified the intensity of the mineral pressure following the pattern of "back ditch section > ditch section > ditch bottom section > normal mining section" [12]. Zhang et al. established

the structural mechanics model of the "unevenly distributed load" of the key layer under the valley terrain and obtained the calculation formula of the "slide rotation load" caused by the instability of adjacent key blocks during the movement of the overlying strata [13].

The aforementioned studies concerning the movement of the overlying strata and mining pressure law under the special topography during the shallow coal mining mainly focus on the naturally developed terrain and trenches [14]. However, due to the upper thin overlying soil layer of the shallow coal, coal outcrop often occurs around the well zone and the gully region, which is often treated with excavation and refilling, resulting in manmade slope around the boundary. Current studies regard the man-made slopes and mining under the man-made slope center around the sliding and instability mechanism and theories during the coordinated open-pit mining. Sun et al. studied the sliding mechanism and deformation mechanism of the combined mining slope of underground and open-pit mining [15, 16]. Ding et al. proposed four stages of slope deformation and failure evolution under the coordinated mining of open wells and revealed the deformation failure mode and instability mechanism of mining slopes under the coupling effect of "key hard rock layers" and "key weak layers" [17, 18]. However, the existing research studies discussing slope slippage, overlying rock movement, and coal pillar stability involved in underground mining of slopes were mainly focused on single-object issues, and few discussions and studies have been performed to explore the coupling interaction among all three factors during the mining process.

Through the theoretical analysis and similar simulations as well as the field tests, this paper discusses the interaction of coal pillar, overlying rocks, and slopes in the same space during the mining process of the manmade slope formed after the excavation and backfilling of the corner coal treatment area. This study is expected to provide some references for mining under similar special mining conditions [19].

2. The Movement Law of the Overlying Strata under the Slope

2.1. Project Background. As a typical loess hilly and gully landform, the Nanliang Coal Mine is featured with a complex topography, some vertical and horizontal gullies, deep ridges and steep ditches, gentle stratum occurrence, shallow coal seams, and simple geological structure.

The working face #30101 locates at the southwest of the mining field. The depth of the coal seam ranges from 80.43 to 112.01 m, with a strike length and dip length of 1398.32 m and 280 m, respectively. Besides, the average thickness of the coal seam is about 2 m. The transportation of the working face is close to the boundary of the minefield along the south side of the channel, which is labelled as the corner coal of 3-1 coal seam. The overlying rock layer is thin with well-developed sandstone fissures, featured with excessive illegal exploration. In order to prevent the surface collapse, the ground fissures from further development, and the illegal exploration in this area, which tends to trigger a spontaneous combustion of the residual coal and 3-1 coal seam goaf, a comprehensive treatment area has been established with a total of $5.05 \times 10^{-2}\,\mathrm{km}^2$ bottom area through the excavation treatment, as shown in Figure 1.

As shown in Figure 2, the bottom of the comprehensive treatment area of 3-1 coal seam and No. 30101-1 working face formed a slope, which was perpendicular to the working face. The slope angle is 53°.

2.2. The Experimental Model Design. During the study of the interaction between the overlying strata, the slope, and the protective pillar during the advancement of the working face under the shallow coal seam slope terrain, a physical simulation method was adopted to simulate the mining process of the 30101-1 working face. In order to minimize the influence of model size, the experiment adopted a geometric similarity ratio of 1 : 100 and established a model of 3 m in length, 0.2 m in width, and 0.9 m in height, as shown in Table 1. Considering that the main material at the pit bottom of the comprehensive treatment area was dominated with the loose loess and gangue, some strata were removed from the comprehensive treatment area and used as the backfill material in the model.

As demonstrated in Figure 3, the spontaneous loads of the overlying strata and slope instability during mining were monitored and recorded via the CL-YB-152 dynamic load data acquisition system which was numbered from left to right starting from 1. A total of 9 displacement detectors were installed above the 3-1 coal seam to monitor the movement of overlying rock and slopes during mining. A number of percentage meters were installed on the surface and in backfill area to monitor surface movement changes during the mining. The development of cracks and fissures during the mining was closely monitored via a BJQF-1 crack width gauge.

2.3. The Movement Features of the Slope during Mining Process. During the simulation, before the mining working force approached the slope, the movements observed during the mining were similar to the movements of the working face during the regular shallow coal mining. The mining triggered the initial fracture in the basic roof and a series of cyclic fractures. The fractured rocks were limited by the lateral horizontal force from the surrounding strata, resulting in a relatively stable hinged structure. No interaction was observed between the overlying strata and the slope during the movements under the mining. The loess layer on the surface was subject to the impacts of the mining face. The fractures caused by the advancement of exploration continued to expand to the surface, forming a fracture face on the vertical profile. The fracture face continued to develop cyclically, approaching to the slope. Simultaneously, the loess on the surface under the advancement of the exploration and the additional stress corresponding to the horizontal deformation caused by the exploration overcome the cohesion or the tensile strength of the soil along with greater deformation in the surface than the depth of the loess. As a result, the fracture on the surface reached the ultimate

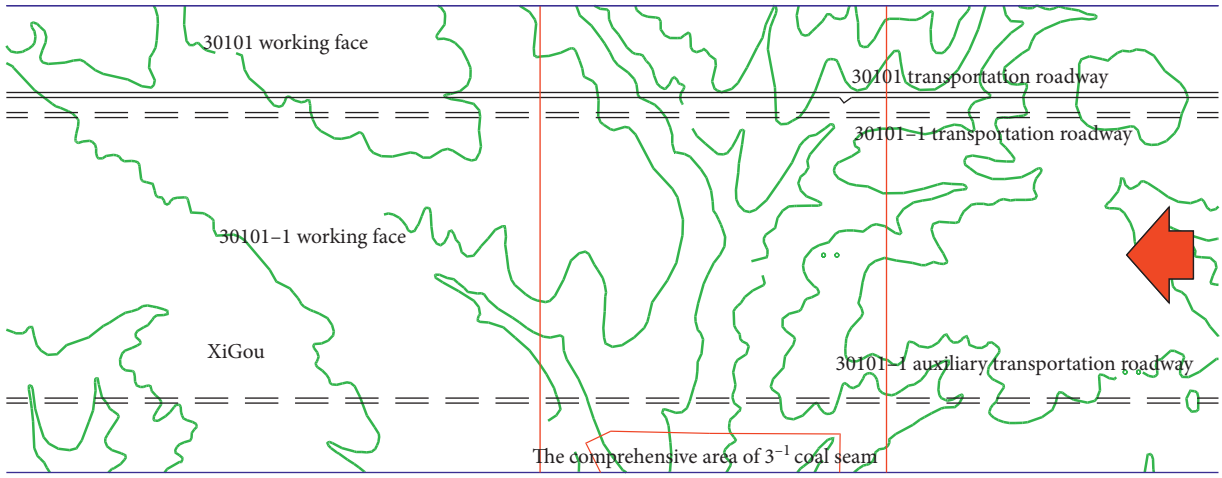

Figure 1: Comparison on surface and underground 30101-1 working face of Nanliang Coal Mine.

Figure 2: Slope body in the comprehensive coal control area of 3-1 coal seam.

Table 1: The material ratio of the model.

Lithology	Thickness (cm)	Material ratio number	Consumable (kg/cm)				
			Sand	Gypsum	Calcium carbonate	Coal ash	Loess
Loess soil	44	20 : 1	9.14	—	—	—	0.45
Medium-grained sandstone	12	737	8.4	0.36	0.94	—	—
No. 2-2 seam	2.5	20 : 1 : 2 : 20	2.0	0.1	0.2	2.0	—
Siltstone	4	837	8.53	0.32	0.75	—	—
Coal streak	0.5	20 : 1 : 2 : 20	2.0	0.1	0.2	2.0	—
Siltstone	12	837	8.53	0.32	0.75	—	—
Fine sandstone	6	746	8.4	0.48	0.72	—	—
Siltstone	5	837	8.53	0.32	0.75	—	—
No. 3-1 seam	2	20 : 1 : 2 : 20	2.0	0.1	0.2	2.0	—
Siltstone	2	837	8.53	0.32	0.75	—	—

equilibrium of the shear failure than that on the deep layers [20]. Details can be viewed in Figure 4.

As the working face approached close to the slope, the overlying strata triggered by the working face impacted the stability of the slope significantly. In simulation, when the distance between the working face and the slope foot was reduced from 20 cm to 18 cm, the slope body was under the impacts of the mining working face. The slope experienced rotation and sliding, with the vector direction pointing to the goaf of the working face. Considering that the backfilling zone was dominated with the loose materials whose resistance to the pressure was nearly zero, the backfilling zone was pressured and squeezed under the structural rotation of the slope, resulting in the heave phenomenon at the bottom of the backfilling zone. The maximum displacement observed at the bottom of the backfilling zone was with a length of 20 mm. The joint between the backfilling zone and slope surface started to develop fissures, resulting in a massive

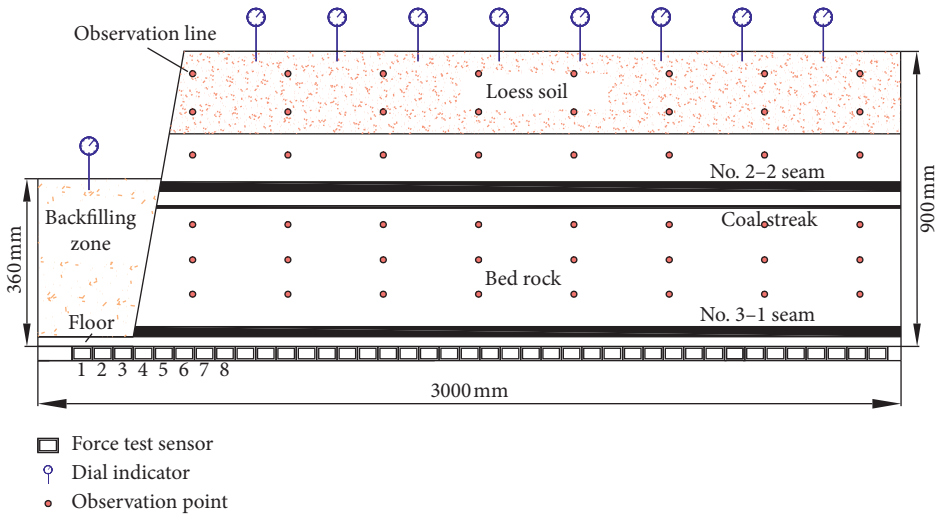

Figure 3: The physical simulation model.

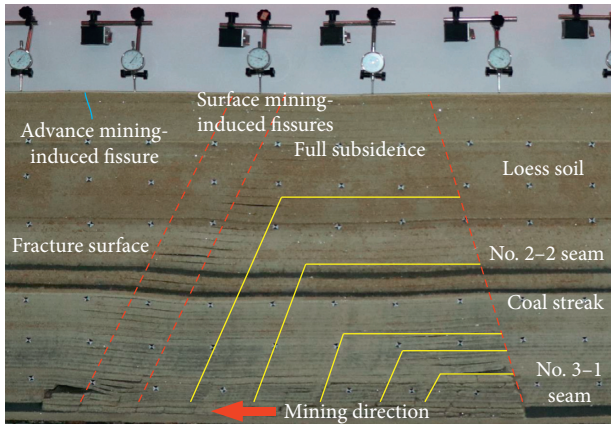

Figure 4: The dynamic development of mining-induced fissures in working face 30101-1.

through crack with an average width of 1.60 mm, allowing the sliding of the slope.

As the simulation indicated, under the circumstance that the working face advanced within the impact range of the slope mining, the slope body tended to develop fissures, slide, and generate bigger cracks under the mining [21]. Along with the cracks before mining, a sliding rotation load structure known as "slope pillar" was formed with the pillar as the main load carrier, as shown in Figure 5. The protective pillar for the slope needs to bear not only the weight of the overlying strata but also the dynamic loading produced during the rotation of the slope toward to the goaf, known as "sliding rotation load" [13]. In the simulation test, when the width of the protective pillar was below 20 cm, the instability of the slope body tended to occur, with the crack surface as the boundary and the inner side of the pillar (close to the working face) as the supporting point to facilitate the process of sliding and rotation. During the movement, the hinged pieces experienced instability and sliding, resulting in the "sliding rotation load" transferred from the back side of the strata to the pillar, which led the load to the inner side of the pillar and dynamic mining pressure [22].

2.4. The Stress Monitoring of the Slope Pillar under Mining. In order to further study the stress variance pattern of the protective coal pillar in different widths, the stress data of the protective pillar collected from the monitoring point 4 to 8 when the working surface was less than 100 m from the slope body were sorted and analyzed (the position of the measuring points is shown in Figure 3). Based on the collected vertical stresses born by the floor collected from the monitoring point 4 to 8 via CL-YB-152 dynamic load data acquisition system, a stress curve is developed and presented in Figure 6. According to Figure 6, as the width of the pillar decreased, the stress monitored at point 4 gradually increased to 3.6 MPa. Under the slope instability, the stress decreased to 3.2 MPa. The stress trend observed at the monitoring point 5 followed a similar pattern. A limited stress increase was observed at the point 5 during the slope instability. The monitoring point 6 was located below the inner side of the slope pillar. As the mining advanced closer to the pillar of the slope, the stress increased accordingly, which continued to rise as high as 5.1 MPa during the slope instability. As the working face advanced to 18 m away from the slope, a hinged rock beam was formed above the working face, resulting in a minimum stress at monitoring point 7. The monitoring point 8 was located behind the working face with a consistent vertical stress, which was still higher than the original stress of the rock.

The analysis of the vertical stresses has suggested that when the width of the protective pillar of the slope was smaller than 20 m, driven by the self-weight, the slope tended to rotate and slide toward the goaf in the same space, resulting in instability. The strata fissures above the goaf zone generated less and less horizontal pushing force, resulting in the occurrence of dynamic load when the slope slid and rotated. The dynamic load was observed at the monitoring point 6 installed in the internal side of the slope pillar, featured with drastic stress increase.

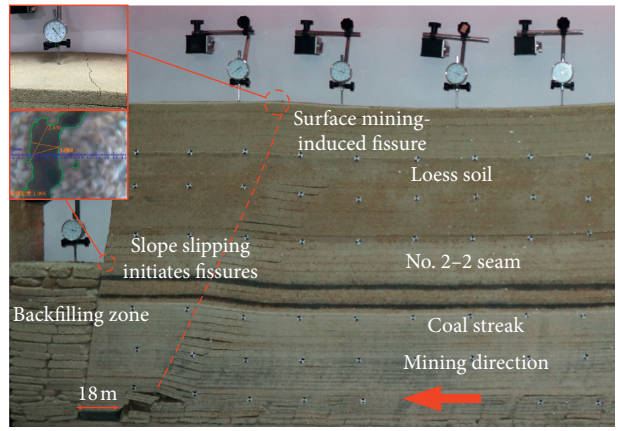

Figure 5: The "slope-pillar" nonuniformly loaded structure.

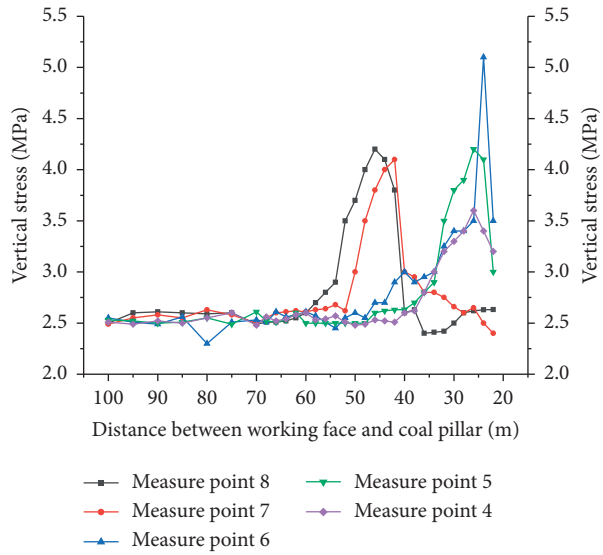

Figure 6: The vertical stress curve established based on the data collected from various monitoring points.

2.5. The Analysis of Nonuniform Load of Slope Pillar. The static load of the protective pillar in the slope area demonstrates a nonuniform trend. Based on previous studies [7, 8, 13, 23], assuming that the structure of the slope is single and the slope angle remains unchanged, following the relationship identified between the protective pillar and the slope projection position, two types of side slope-pillar mechanical models have been established, as shown in Figure 7. In Figure 7, F_1 refers to the supporting force of the external side of the pillar to the overlying strata, F_2 refers to the supporting force of the internal side of the slop pillar to the overlying strata, and F_3 refers to the supporting force for broken block.

The width of the slope pillar is equal to or greater than the horizontal projection length of the slope, as shown in Figure 7(a). According to the structural mechanics, taking the supporting point of the outside of pillar as the point O as the research object, it is concluded that

$$P_a \cdot \frac{2}{3}a + P_b\left(a + \frac{1}{2}b\right) = F_2 \cdot a + F_3 \cdot (a + b). \quad (1)$$

Taking the internal side of the pillar as the supporting point, the following equation can be obtained:

$$P_a \cdot \frac{1}{3}a + F_3 \cdot b = F_1 \cdot a. \quad (2)$$

In formula (3), P_a refers to the nonuniform distribution load, and P_b stands for the uniform distribution load, which can be calculated according to formula (4).

$$P_a = \rho g \cdot v_a, \quad (3)$$

$$P_b = \rho g \cdot v_b. \quad (4)$$

ρg refers to the average body force of the overlying rock layer of the key layer, KN/m^3; v_a indicates the volume of the overburden with nonuniform load, $v_a = 0.5a^2\tan\alpha$ (α the slope angle of toe); v_b is the volume of overlying strata with uniform load; and a suggests the width of the slope pillar, m;

The width of the slope pillar is less than the horizontal projection length of the slope, as shown in Figure 7(b). According to the structural mechanics, taking the supporting point of the outside of pillar as the point O as the research object, it is concluded that

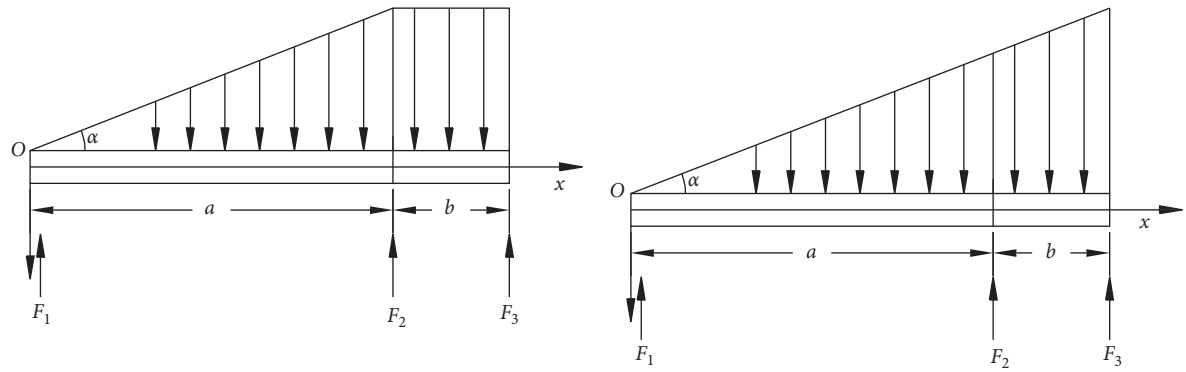

Figure 7: Force diagram of nonuniform load pillar.

$$P_a \cdot \frac{2}{3}(a+b) = F_2 \cdot a + F_3 \cdot (a+b). \tag{5}$$

Taking the internal side of the pillar as the supporting point, the following equation can be obtained:

$$P_a \cdot \frac{1}{3}a + F_3 \cdot b = F_1 \cdot a. \tag{6}$$

When the broken block slips and loses stability, F_1 and F_2 can be calculated by formulas (1), (2), (5), (6).

$$\begin{cases} F_2 = P_a \cdot \dfrac{2}{3}a + P_b\left(a + \dfrac{1}{2}b\right), \\ F_1 = P_a \cdot \dfrac{1}{3}, \end{cases} \tag{7}$$

$$\begin{cases} F_2 = P_a \cdot \dfrac{2}{3a}(a+b), \\ F_1 = P_a \cdot \dfrac{1}{3}. \end{cases} \tag{8}$$

When the slope pillar is unstable, based on the analysis of the movement features of the slope during mining process and the stress monitoring results of pillar, the protective pillar for the slope needs to bear both the weight of the overlying strata and the instantaneous slipping and rotating load F_h produced during the rotation of the slope toward to the goaf.

$$F_h = \phi G_B \tan\delta. \tag{9}$$

In formula (9), φ refers to the instantaneous impact coefficient; δ indicates the rotation angle; and G_B is the overburden load above the slop pillar.

According to (7) and (8), under the action of the static load of the side slope, the load on the internal side of the pillar is greater than that on the external side of the pillar. When the pillar is not affected by the instantaneous slip and rotation load, the pillar only bears the load of the overlying rock layer and the instability failure of $F_1 > R$ coal pillar under static load (R is the ultimate strength of the coal pillar). When the pillar is affected by the instantaneous slipping and rotating load, the pillar needs to bear not only the static load of the overlying rock but also the instantaneous slipping and rotating load, resulting in $F_1 + F_h < R$, which suggests that the pillar is likely to undergo instantaneous slipping load instability and failure.

3. The Stability Analysis of the Protective Pillar of Slope

According to the "slope-pillar" unevenly distributed load structure dominated by the pillar as the main load bearer, obtained from the simulation (combined with the research results of reference [16, 24, 25]), a "slope-pillar" structural mechanical model was established to analyze the stability of the pillar of the slope, as demonstrated in Figure 8.

As demonstrated in Figure 8, the fissure face AB and premining fissure BE jeopardized the integrity of the slope, resulting in the development of characteristics of double slip surfaces in the slope and stability reduction. Due to the loess and gangue used in the backfilling zone III, the slope reinforcement was limited. Without considering the hydraulic effect and the reinforcement of backfilling zone to the slope foot, the length of the slip surface formed by the width of the pillar and the length of the broken section determine the slope stability [26, 27].

According to the slope structure, the length, inclination, cohesion, and internal friction angle of AB are designated by L_1, β_1, c_1, and φ_1, respectively. The length, inclination, cohesion, and internal friction angle of BC are designated by L_2, β_2, c_2, and φ_2, respectively. DC refers to the slope surface with a slope angle α.

Assuming after point B, the inclined angle θ between the shear surface of the soil body of the mining and the surface of the maximum principal stress created a boundary surface BE which divided the slope body into part I and II, corresponding to weight W_1 and W_2. The detailed calculation of W_1 and W_2 is listed in the following formula:

$$\begin{cases} W_1 = \dfrac{1}{2}\gamma H^2(\cot\theta + \cot\beta_1), \\ W_2 = \dfrac{1}{2}\gamma H(2L_2 - H\cot\alpha - H\cot\theta \end{cases} \tag{10}$$

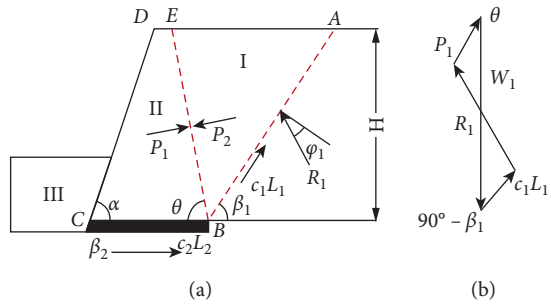

Figure 8: The schematic diagram of structural stability analysis of "slope pillar."

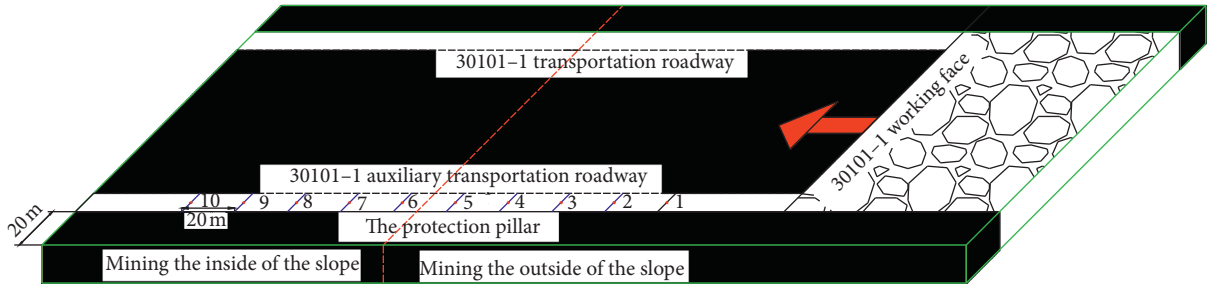

Figure 9: The comprehensive measuring monitoring station layout plan.

Due to the instability and sliding of the fissure blocks in the overlying strata during the slope instability, the horizontal pushing force toward the slope can be overlooked [25]. Assuming that no additional external force working on the slope, the friction from the bedrock imposed on the slope part I can be calculated as follows:

$$R_1 = W_1 \cos\beta_1 \sqrt{1 + \tan^2\phi_1}. \tag{11}$$

P_1 and P_2 refer to the interaction force between part I and part II, respectively, which equals to each other with opposite direction. P_1 can be calculated as follows:

$$P_1 = \frac{R_1 \sin\beta_1 - c_1 L_1 \cos\beta_1}{\sin\theta}. \tag{12}$$

The slope safety coefficient F is defined as the ratio between the sliding resistance force of the slope structural face and sliding force, which means F is the sliding resistance force/sliding force [25], which leads to the calculation formula of slope safety coefficient F_2 for part I.

$$F_2 = \frac{W_2 \cos\beta_2 \tan\phi_2 + P_2 \cos(\theta + \beta_2)\tan\phi_2 + c_2 L_2}{W_2 \sin\beta_2 + P_2 \sin(\theta + \beta_2)}. \tag{13}$$

Because $\beta_2 = 0°$, the calculation formula of slope safety coefficient F_2 for part II is developed and presented in the following formula:

$$F_2 = \frac{W_2 \tan\phi_2 + P_2 \cos\theta \tan\phi_2 + c_2 L_2}{P_2 \sin\theta}. \tag{14}$$

According to the force analysis conducted previously, the safety coefficient of part I was obtained under the extreme equilibrium. Assuming the slope body is a rigid structure as a whole, $F = F_1 = F_2 = 1$ can be obtained.

$$F_2 = \frac{W_2 \tan\phi_2 + P_2 \cos\theta \tan\phi_2 + c_2 L_2}{P_2 \sin\theta} = 1. \tag{15}$$

According to formula (15), the width of pillar of the slope under the slope extreme equilibrium can be calculated based on the following formula:

$$L_2 = \frac{1}{c_2}\left[P_2 \sin\theta - W_2 \tan\phi_2 - P_2 \cos\theta \tan\phi_2\right]. \tag{16}$$

Since $P_1 = P_2$,

$$L_2 = \frac{1}{c_2}\left[P_1 \sin\theta - W_2 \tan\phi_2 - P_1 \cos\theta \tan\phi_2\right]. \tag{17}$$

According to the corresponding conditions of Nanliang No. 30101-1 working face, the following data were obtained: $\alpha = 80°$, $\beta_1 = 60°$, $\beta_2 = 0°$, $\theta = 45 + \varphi/2$, $c_1 = c_2 = 1 \times 10^3$ kpa, $\varphi_1 = \varphi_2 = 25°$, $\gamma = 25$ KN/m^3, and $H = 56$ m.

Applying the corresponding data listed above into formulas (10), (11), (12), and (17), the width of the pillar is calculated as follows:

$$L_2 = 19 \cdot 64 \text{ m}. \tag{18}$$

According to the actual dimensional requirements in the field, the width of the retention pillar cannot be less than 20 m.

4. Engineering Validation

To further verify the validity of the formula developed and listed in the previous section, a total of 10 comprehensive measuring stations were set up in the auxiliary transportation roadway of No. 30101-1 working face in Nanliang Coal Mine. Each measuring station was 20 m apart. The

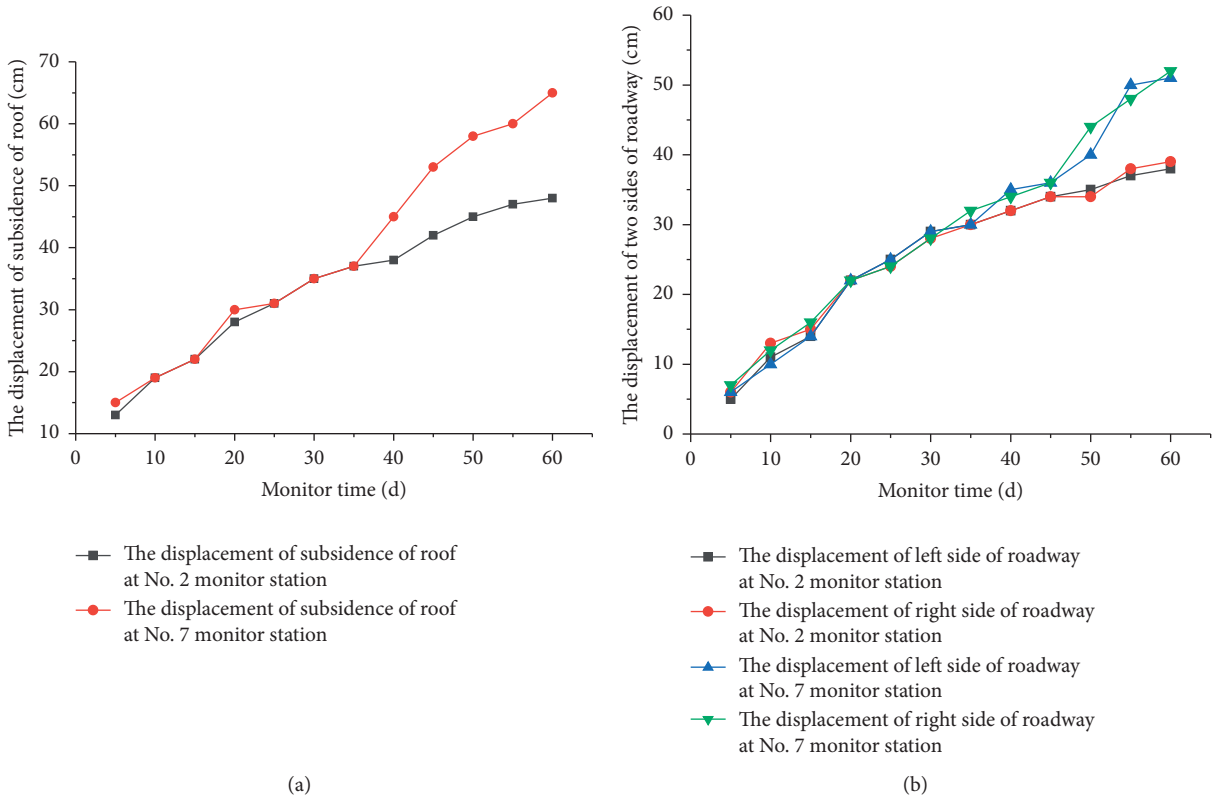

Figure 10: Displacement of surrounding rock of haulage roadway: (a) the subsidence of the roof; (b) the lateral displacements of the roadway.

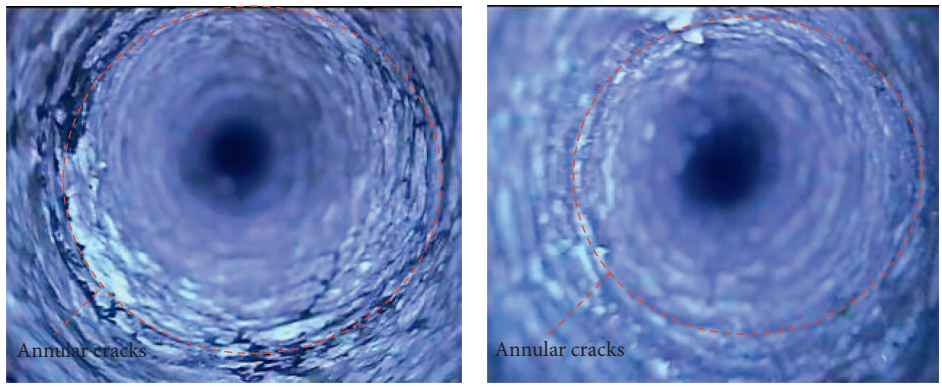

Figure 11: The peep results from the No. 2 monitor station: (a) 30 cm; (b) 75 cm.

measurement stations 1 to 5 were set in the lower section of the nonslope roadway, and the measurement stations 6 to 10 were set in the lower section of the slope roadway. The measurement station layout is illustrated in Figure 9. The comprehensive measuring station adopts the cross-point method, and the CXK-12 mine intrinsically safe borehole imager method was adopted to monitor the approaching amount of the two sides and the amount of roof subsidence of the 30101-1 auxiliary transportation roadway and the degree of damage to coal pillar when the working face passes the slope and the nonslope during the mining process.

After analyzing the collected data of the surrounding rock displacement of the roadway, the curves between the working face advancing distance and the subsidence of the roof of the mining roadway and the displacement of the both sides of roadway, respectively, were obtained, as shown in Figure 10. Comparing the roadway roof subsidence and the displacement in both sides of roadway between the slope section and nonslope section, it is revealed that the deformation of the surrounding rock in the slope section is larger than that in the corresponding nonslope section. The maximum difference of the roadway floor subsidence

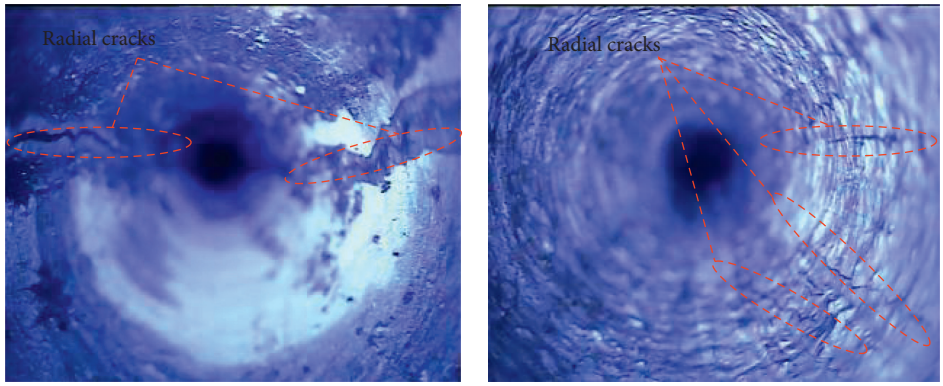

(a) (b)

Figure 12: The peep results from the No. 7 monitor station: (a) 30 cm; (b) 83 cm.

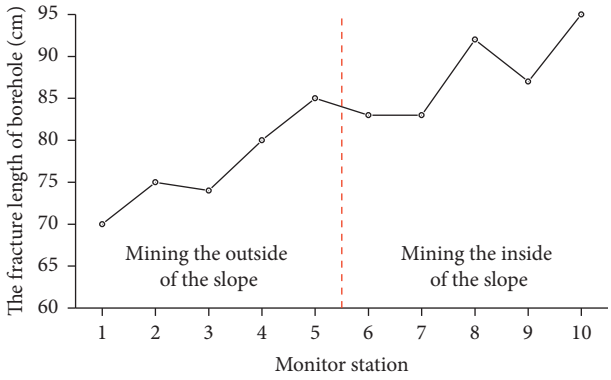

Figure 13: The peep borehole fracture development location line diagram.

reached 17 cm with 14 cm as the maximum displacement difference at the roadway sides. It is worth mentioning that the deformation of the roadway surrounding rock was all within the controllable range.

Holes were drilled to gain some glimpses of one side of the protective pillar to analyze the damage process of the pillar and coal body when the returning working face was 30 m away. Due to the length limitation of this study, only the screenshots of the observation effects of No. 2 and No. 7 boreholes are included in the paper. The front and back ends of the boreholes of No. 2 and No. 7 are presented in Figures 11 and 12, respectively. From Figures 11 and 12, the inner wall of the borehole was relatively intact, and the borehole did not show any severe deformation, block loss, hole collapse, and so on. The borehole wall of No. 2 was mainly developed with annular cracks, and the borehole wall of No. 7 was dominated with the radial cracks. The crack depth was greater than the depth of No. 2 borehole. The obtained results of the boreholes at each station were collected to develop the broken line diagram of the crack development position, as shown in Figure 13. Before the mining face advanced to the slope, the maximum depth of cracks in the borehole was 85 cm with an average depth of 76.8 cm. After the mining face advanced into the slope, the maximum depth of cracks in the borehole reached 95 cm with an average depth of cracks of 88 cm, demonstrating increased crack depths with limited variances in fragmentation.

The analysis reveals that when the width of the protective pillar of the slope reaches 20 m, the deformation of the roadway surrounding rocks under the influence of the mining within the slope tends to increase at an acceptable safety level, with deeper cracks developed in the pillar. However, the fragmentation in the pillar is limited without jeopardizing the stability of the pillar and no dynamic load instability occurred in the coal pillar. The result can meet the safety requirements on-site.

5. Conclusion

(1) The simulation has revealed that as the working face advanced and the width of the slope protective pillar reached the boundary width, the "slope-pillar" structure formed by the slope, pillar, and fissure face tended to experience rotation, sliding, and instability. The concentrated stress points were identified at the slope foot. Eventually, the cracks grew, forming a massive through fissure. The backfilling zone was pressured and squeezed by the "slope-pillar" structure, resulting in an increased stress and the rib spalling on the pillar.

(2) Through similarity simulation on the movement of slope strata and the monitoring on pillar stress during mining process, a mechanical model of nonuniform loading of "slope pillar" was established, which demonstrated that the rotation slip of the overlying strata of the slope under the limit equilibrium condition was a contributing factor to the dynamic load instability of the "slope pillar." The criterion for judging the dynamic load instability of the "slope pillar" was given as $F_1 + F_h < R$.

(3) A "slope-pillar" mechanical model was established along with the boundary width calculation formula for the "slope-pillar" structure under extreme equilibrium. The formula was used to calculate the minimum 20-meter width of the protective pillar for No. 30101-1 working face in Nanliang mining zone.

(4) The engineering validation indicated that when the width of the protective pillar reached 20 meters, the average cracks depth inside the pillar was 88 cm, no dynamic load instability occurred, and the deformation of the roadway surrounding rock was all within the controllable range, which also further reflected the validity of the boundary width formula for the pillar under the extreme balance conditions.

Data Availability

The data used to support the findings of this study are available from the corresponding author upon request.

Conflicts of Interest

The authors declare that they have no conflicts of interest.

Acknowledgments

The research was funded by the National Natural Science Foundation of China (nos. 51774229 and 52004204), the Innovation Capacity Support Program (Science and Technology Innovation Team) of Shaanxi Province (no. 2018TD-038), the Natural Science Fundamental Research Program-Joint Fund Project of Shaanxi Province (no. 2019JLM-41), and the Open Fund Project of State Key Laboratory for Water Resources Protection and Utilization in Coal Mining (no. SHJT-17-42.3).

References

[1] P. W. Shi and Z. J. Hou, "Law of roof breaking movement of shallow seams in ShenFu cam," *Journal of Xi'an Mining Institute*, vol. 16, no. 3, pp. 204–207, 1996.

[2] Z. J. Hou, "The criterion on determining main roof in breaking zone and its application to the shallow seam," *Journal of China Coal Society*, vol. 28, no. 1, pp. 8–12, 2003.

[3] J. L. Xu, W. B. Zhu, X. Z. Wang, and M. S. Yi, "Classification of key strata structure of overlying strata in shallow coal seam," *Journal of China Coal Society*, vol. 34, no. 7, pp. 865–870, 2009.

[4] Q. X. Huang, *Study on Roof Structure and Strata Control of Shallow Coal Seam Longwall Mining*, China University of Mining and Technology Press, Xuzhou, China, 2018.

[5] M. G. Qian, P. W. Shi, and J. L. Xu, *Mine Pressure and Rock Formation Control*, China University of Mining and Technology Press, Xuzhou, China, 2010.

[6] J. Zhang and Z. J. Hou, "Failure rule of overburden movement in shallowly buried coal seam covered with thick soils," *Journal of Mining & Safety Engineering*, vol. 24, no. 1, pp. 56–59, 2007.

[7] X. F. Wang, D. S. Zhang, X. Lu et al., "Strata behavior features of shallow depth thin seam mining under sand-soil gully slope," *Coal Science and Technology*, vol. 38, no. 6, pp. 18–22, 2010.

[8] Z. Q. Zhang, *Study on Influence Law of Dynamic Strata Pressure in the Shallow Coal Seam Face under Hilly and Gully Terrain*, China University of Mining and Technology, Xuzhou, China, 2011.

[9] Y. J. Liu, Q. J. Qi, and A. H. Wang, "Influence of valleys terrain on pressure of fully mechanized working faces in shallow coal seams," *Shock and Vibration*, vol. 2021, Article ID 8880041, 11 pages, 2021.

[10] H. Z. Wang, H. Liu, S. S. Song, and Y. Chen, "Study on ground pressure behaviors of working face in nearly shallow coal seam under gully terrain," *China Mining Magazine*, vol. 29, no. 9, pp. 116–120, 2020.

[11] G. L. Hu, W. B. Zhu, X. J. Wang, and Z. J. Zhang, "Influencing mechanism of gully terrain on ground pressure behaviors in shallow seam longwall mining," *Journal of China Coal*, vol. 37, no. 2, pp. 179–185, 2012.

[12] F. T. Wang, S. H. Tu, W. Y. Zhang, Q. Song, R. Yan, and C. Duan, "Ground pressure rules and roof control technology for the longwall mining of shallow seam beneath the gully topography," *Journal of Mining & Safety Engineering*, vol. 32, no. 6, pp. 877–882, 2015.

[13] J. Zhang, J. J. Long, T. Yang et al., "Study on dynamic loading mechanism of mining in gully area of shallow coal seam," *Journal of Mining & Safety Engineering*, vol. 36, no. 6, pp. 1222–1227, 2019.

[14] G. W. Fan, D. S. Zhang, and X. F. Wang, "Mechanism of roof shock in longwall coal mining under surface gully," *Shock and Vibration*, vol. 2015, Article ID 803071, 8 pages, 2015.

[15] S. G. Sun, M. F. Sun, and J. S. Wang, "Effect of combined underground and open pit mining and deformation mechanism of slope," *Chinese Journal of Rock Mechanics and Engineering*, vol. 18, no. 5, pp. 497–502, 1999.

[16] S. G. Sun, M. F. Sun, and J. S. Wang, "Study on of sliding mechanism for slope due to the excavation from open pit into underground mining," *Chinese Journal of Rock Mechanics and Engineering*, vol. 19, no. 1, pp. 126–129, 2000.

[17] X. P. Ding, J. Wang, W. Li et al., "Analysis of slope sliding depth for open-underground combined mining under coupling effects about key strata," *Journal of China Coal*, vol. 39, no. S2, pp. 354–358, 2014.

[18] X. P. Ding, Z. W. Wang, and W. Li, "Dynamic process and typical deformation-failure mechanism of mining slope," *Journal of China Coal*, vol. 41, no. 10, pp. 2606–2611, 2016.

[19] Z. C. Cai, *The Research of Slope Protect Coal Pillar Reservation and protection of Combining Open-Pit with Underground Mining*, Liaoning Technology University,, Fuxin, China, 2009.

[20] J. Li and C. Y. Liu, "Formation mechanism and reduction technology of mining-induced fissures in shallow thick coal seam mining," *Shock and Vibration*, vol. 2017, Article ID 1980817, 14 pages, 2017.

[21] Z. G. Tao, M. N. Li, C. Zhu, M. He, X. Zheng, and S. Yu, "Analysis of the critical safety thickness for pretreatment of mined-out areas underlying the final slopes of open-pit mines and the effects of treatment," *Shock and Vibration*, vol. 2018, Article ID 1306535, 8 pages, 2018.

[22] Z. Sun, Y. Z. Wu, Z. G. Lu, Y. Feng, X. Chu, and K. Yi, "Stability analysis and derived control measures for rock surrounding a roadway in a lower coal seam under concentrated stress of a coal pillar," *Shock and Vibration*, vol. 2020, Article ID 6624983, 12 pages, 2020.

[23] N. Jiang, D. Yin, J. B. Ma, L. Han, H. Pan, and Q. Yin, "Effects of water immersion on the long-term bearing characteristics of crushed gangue in goaf," *Geofluids*, vol. 2021, Article ID 6675984, 11 pages, 2021.

[24] J. M. Zhu, B. K. Liu, J. H. Xu et al., *Open-Pit and Underground Combined Mining Technology*, China University of Mining and Technology Press, Beijing, China, 2009.

[25] S. J. Liu, M. W. Guo, and C. H. Liu, "Calculation of residual sliding force of slop based on finite element method," *Chinese*

Journal of Rock Mechanics and Engineering, vol. 36, no. S2, pp. 4054–4065, 2017.

[26] Z. Yu, Y. T. Zhi, and L. Qing, "Slop stability analysis using slice-wise factor of safety," *Mathematical Problems in Engineering*, vol. 2014, Article ID 712145, 6 pages, 2014.

[27] R. Wang, S. Yan, J. B. Bai, Z. Chang, and T. Zhao, "Theoretical analysis of damaged width & instability mechanism of rib Pillar in open-pit highwall mining," *Advances in Civil Engineering*, vol. 2019, Article ID 6328702, 15 pages, 2019.